Thermophotovoltaic Converter Performance for Radioisotope Power Systems

Christopher J. Crowley[1], Nabil A. Elkouh[1], Susan Murray[2], Donald L. Chubb[3]

[1]*Creare Inc., P.O. Box 71, Hanover, NH 03755*
[2]*Emcore Corporation, 10420 Research Road SE, Albuquerque, NM 87123*
[3]*NASA Glenn Research Center, 21000 Brookpark Road, Cleveland, OH 44135*
603-643-3800, cjc@creare.com

Abstract. The development of lightweight, efficient power for emerging NASA missions and recent advances in thermophotovoltaic (TPV) conversion technology have renewed interest in combining radioisotope heat sources with photovoltaic energy conversion for Radioisotope Power Systems (RPS) for spacecraft. TPV power conversion uses advanced materials able to utilize a broader, spectrally tuned range of wavelengths for more efficient power conversion than Si solar cells. Spectral control, through choices of selective radiant emitters, TPV modules, and filters, is key to high-efficiency operation. This paper describes performance tests of an array of TPV cells with boundary conditions prototypical of an RPS. TPV performance tests were conducted at prototypical array size (≅100 cm^2), emitter temperature (1350 K), and heat rejection temperature (300 K). Test hardware included InGaAs TPV cells at 0.60 eV band-gap, with tandem plasma/interference filters for spectral control. At the target emitter temperature of 1350 K, a conversion efficiency of 19% has been demonstrated for the TPV module. Results are consistent with measured cell efficiency (28%), calculated spectral control efficiency (80%), and calculated thermal efficiency in the optical cavity (90%).

INTRODUCTION

The context of the work described in this paper is radioisotope power systems (RPS) for spacecraft. Many space missions are to places where solar power cannot be used because the location is too distant from the sun, or lying in shadow much of the time. For those missions, NASA has used nuclear heat sources with thermal-to-electric converters to generate the power required by the spacecraft. Since the 1960's, NASA has launched 42 radioisotope thermoelectric generators (RTGs) on 25 spacecraft. The RTG systems are characterized by using the heat of decay from radioactive plutonium (Pu^{238}) coupled with thermoelectric converters to generate the electrical power.

To generate 300 W of electrical power for the Cassini mission, for example, each RTG has a stack of 18 General Purpose Heat Source (GPHS) units. The 4500 W of power from these heat sources generates the ≅ 300 W of electric power using thermoelectric power conversion at ≅ 8%. The power conversion efficiency for the RTG system is only about 7%, and the specific power is about 4.5 W_e/kg.

NASA is currently sponsoring R&D related to advanced technology for power conversion. The purpose of this forward-looking program is to develop the means to increase power for spacecraft efficiently, thereby fundamentally increasing NASA's capability for exploration of the outer Solar System. As part of this program, NASA is funding a variety of research and development projects under NASA Research Announcement 02-OSS-01, "Radioisotope Power Conversion Technology." New approaches being explored encompass various power conversion technologies, including dynamic systems such as Stirling and Brayton cycles and static systems such as thermophotovoltaics (TPV) and advanced thermoelectrics (TE). These technologies are expected to improve the conversion efficiency and the specific power of RPS by factors of two to four.

This paper addresses TPV power conversion. Seminal papers on radioisotope power systems with TPV power conversion were presented in 1995 and 1996 (Loughlin and Uppal, 1995; Schock and Or, 1996; and Vicente, *et al.*, 1996). Basic system hardware concepts have been presented, as well as performance calculations. With renewed interest in TPV based upon advances in the performance of TPV cells, more recent papers (DePoy, *et al.*, 2003;

CP746, *Space Technology and Applications International Forum—STAIF 2005,* edited by M. S. El-Genk

Fraas, *et al*., 2003) provide updated performance estimates. The focus of current investigations is the efficiency of TPV power conversion. The unique aspects of this paper are the experimental performance data under prototypical boundary conditions, with advanced TPV cells and spectral control.

RADIOISOTOPE POWER SYSTEM CONCEPT

As a reference for the following discussion, Figure 1 illustrates one conceptual design approach for an RPS using two GPHS units with TPV power conversion. This basic concept for a 500 W_t system is described by Schock, Or, and Kumar (1996). This system incorporates two GPHS units, or a cube ~10 cm (~4 inches) on a side. The GPHS units are supported in a canister. The canister is in turn enclosed by an aluminum housing assembly. Piston/nut assemblies with zirconia balls are used to support the canister in the housing and to minimize parasitic heat losses at the same time. Multifoil insulation in the housing minimizes parasitic heat losses.

The TPV converters are located on each of the two end faces of the housing. Each face is about 100 cm^2. The actual surface area to be occupied by the TPV cells on this face opposite the heat source is a design variable. Key boundary conditions in this design are:

- The range of operating temperature on the outer surface of the aeroshell is limited between 1200 K and 1350 K to keep the iridium cladding on the fuel pellets within acceptable limits. The temperature constraints set important limits on the design.
- Since the power input is 500 W_t in each of two faces at 100 cm^2 area, the heat flux on each TPV array is about 2.5 W/cm^2, assuming that the other faces are well insulated.

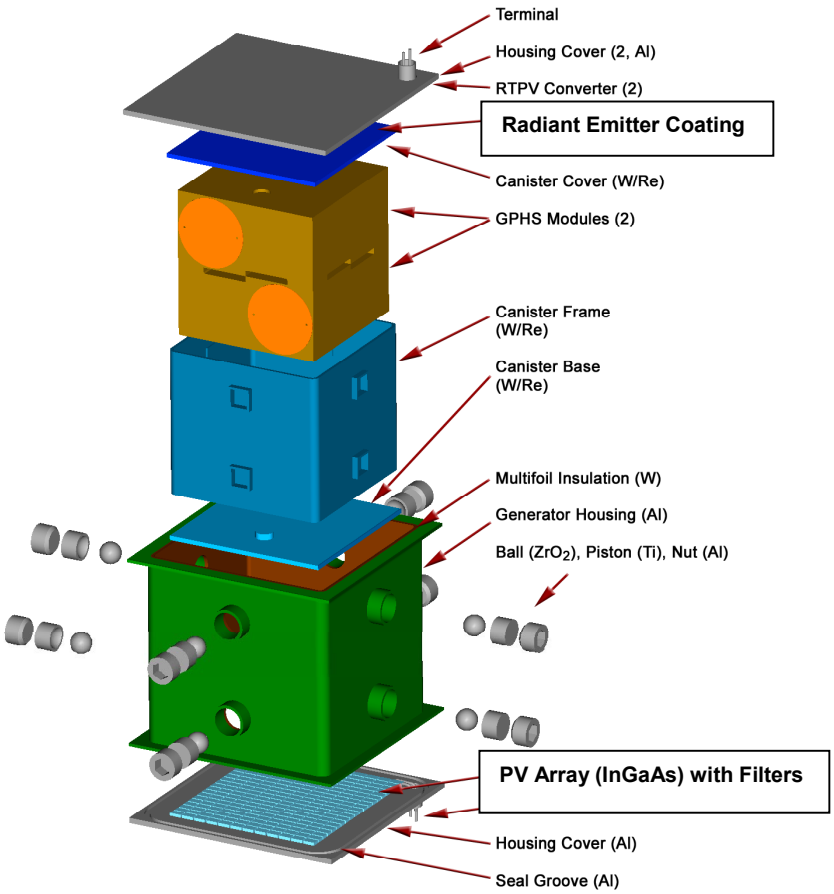

FIGURE 1. RPS System Concept with TPV Power Conversion.

THERMOPHOTOVOLTAIC (TPV) BASICS

Thermophotovoltaics converts the radiant heat from the GPHS heat source to electricity. Figure 2 illustrates the TPV conversion process. A hot emitter surface (at a temperature of 1200 K to 1350 K in this case) emits radiation. The power of the emitted radiation varies with wavelength. A filter component provides spectral control. The filter facilitates transmission of radiation in (shorter) wavelengths usable by the TPV cells and reflects radiation in (longer) wavelengths unusable by the TPV cells. The TPV cell converts a portion of the transmitted radiation to electricity. The remaining portion of the transmitted radiation is rejected to a heat sink, via radiators on the spacecraft.

Figure 3 illustrates the most important features of the TPV conversion process. Understanding these features provides a first-order understanding of TPV power conversion. For a TPV cell at a band-gap E_g = 0.60 eV, the critical wavelength is λ_c = 2.07 μm. The "Quantum Efficiency" line in Figure 3 indicates the quantum efficiency of a TPV cell at this band-gap, showing that it can convert photons at wavelengths between 1 and 2.07 μm efficiently.

TPV Cell Efficiency. Focusing first upon the portion of Figure 3 at λ_c < 2.07 μm, the "Power Density of Black Body Emitter" line shows the normalized power density for a black-body (ε = 1.0) radiant emitter at 1350 K. This black-body result is the maximum energy density that can be provided by the radiant emitter. The "Power Density with Spectral Control" line shows the normalized power density for an emitter with an emittance about half that of a black-body radiant emitter, or ε ≅ 0.5, with a tandem filter. In this range, the emitter controls the power density; the filter has a second-order effect because it is highly transmissive in this range, not reflecting or absorbing a significant amount of energy. The total in-band power density in the range of wavelengths that can be converted by the TPV cells is the Area A under the "Power Density with Spectral Control" line in the plot. Of this power, the TPV cell converts a fraction of this energy to useful electrical power. The Area C under the "Power Out" line in Figure 3 represents the useful power. The efficiency of the TPV cell is then the ratio of the Area C to Area A. This cell efficiency is about $\eta_{PVcell} \cong 30\%$ for the InGaAs MIMs on this project.

Spectral Efficiency. Now focus upon the portion of Figure 3 at λ_c > 2.07 μm. In this range, the line "Power Density of Black Body Emitter" once again shows the power density that would emanate from a black-body radiant emitter. Because this power cannot be converted to useful electrical power by the TPV cell, it is desired to minimize the power density to the TPV cells in this range. That is the role of the filter. In this range, the reflectance of the filter controls the power density, and the emittance of the radiant emitter matters only to second-order. The portion of the "Power Density with Spectral Control" line at λ_c > 2.07 μm represents the out-of-band power density with the tandem filters used on this project. The Area B under this line represents the total power density delivered to the TPV cells in this range. The total power density in the TPV converter, or the net heat flux in the optical cavity, is then the sum of Area A plus Area B in Figure 3. With the tandem filter, the in-band Area A is much larger than the out-of-band Area B.

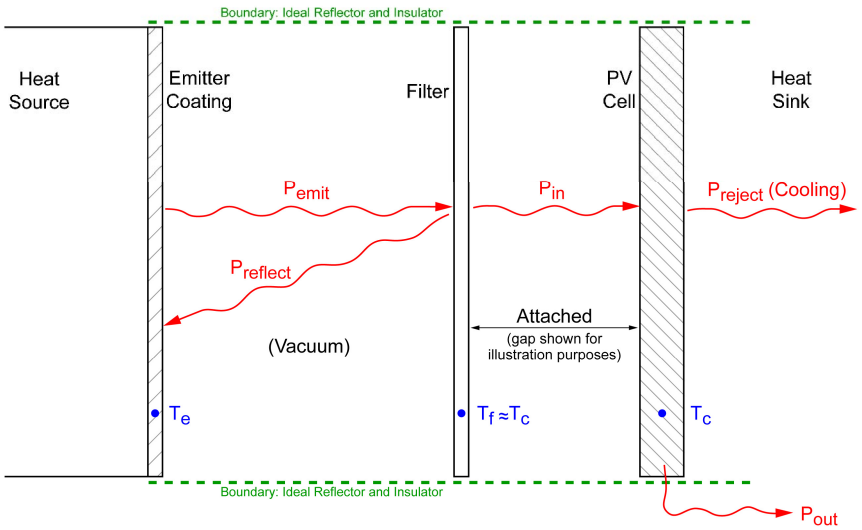

FIGURE 2. Thermophotovoltaic Power Conversion Process.

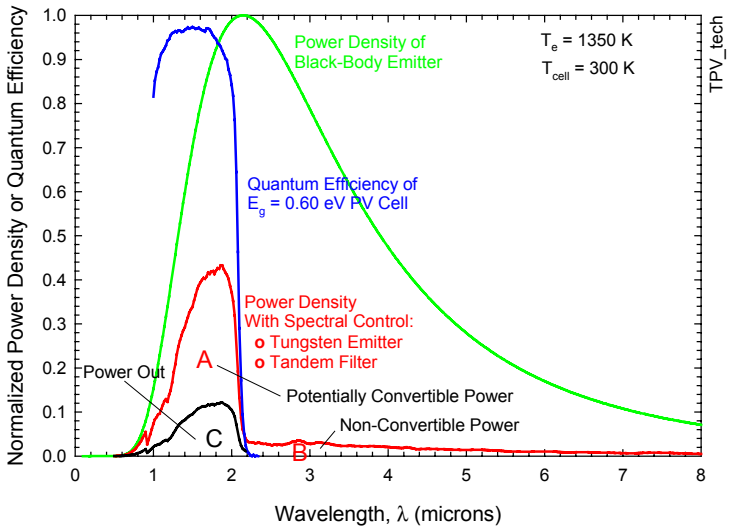

FIGURE 3. Key Spectral Considerations for TPV Converters.

Therefore, the emittance of the radiant emitter primarily determines the heat flux in the optical cavity. We define the spectral efficiency of the TPV converter as the ratio of in-band power (Area A) to total power (Area A plus Area B). With a tandem filter, this spectral efficiency is $\eta_{spectral} \cong 80\%$.

TPV Conversion Efficiency. The efficiency of the TPV converter with a tandem filter is then:

$$\eta_{RTPV} \cong (\eta_{PVcell})(\eta_{spectral}) \cong (30\%)(80\%) \cong 24\% \tag{1}$$

Without a tandem filter, the conversion efficiency is about 15% because the spectral efficiency of the TPV cells is $\eta_{spectral} \cong 50\%$. As discussed later, these values have been confirmed by tests with single TPV cells facing a radiant emitter at about 1350 K.

While the TPV cell efficiency and the spectral efficiency are the dominant effects, in a practical RPS which has a fixed heat input, the net electrical power output and conversion efficiency that are realized will also depend upon other factors, including parasitic heat losses, spatial distributions of temperature leading to non-uniform illumination on the TPV cell arrays, the parallel/series network configuration of the TPV cells in arrays, non-uniform temperatures of the TPV cell arrays, and losses during power-conditioning. The net conversion efficiency can be broken down into a number of components representing these effects:

$$\eta_{RTPV} = (\eta_{housing}) \times [\ (\eta_{cavity}) \times (\eta_{spectral}) \times (\eta_{PVcell}) \times (\eta_{network})] \times (\eta_{DCcontrol}) \tag{2}$$

$$\left(\frac{P_{net,cavity}}{P_{source}}\right)\left(\frac{P_{total,PVcells}}{P_{net,cavity}}\right)\left(\frac{P_{in-band}}{P_{total,PVcells}}\right)\left(\frac{P_{PVcell,electrical}}{P_{in-band}}\right)\left(\frac{P_{array}}{P_{PVcell,electrical}}\right)\left(\frac{P_{28VDC}}{P_{array}}\right) \tag{3}$$

The test results with the array of 16 TPV cells as reported here include the following loss factors:

$$\eta_{array} = [\ (\eta_{cavity}) \times (\eta_{spectral}) \times (\eta_{PVcell}) \times (\eta_{network})\ ] \tag{4}$$

which represent parasitic losses in the optical cavity, spectral efficiency, cell efficiency, and electrical losses in the array due to non-uniform illumination. Separate, supplementary tests have been performed to measure the efficiency of single TPV cells without filters (η_{PVcell}) and single-TPV cells with filters ($\eta_{spectral}$ x η_{PVCell}). The effects of $\eta_{housing}$ and $\eta_{DCcontrol}$ are not yet included in the present testing, but can be estimated analytically. We plan to address these other two factors experimentally in future work.

TEST PARAMETERS AND TPV COMPONENT HARDWARE

Table 1 lists the design parameters and ranges of interest to TPV power conversion. Our test is intended to represent the baseline design with TPV arrays on two sides. Each array has A_{array} ~100 cm^2 area and a heat flux of up to P_{in} = 2.5 W/cm^2. In each test, the temperature of the radiant emitter is varied in the range of T_e = 1100 K to 1400 K, with 1350 K being the design target, and the heat rejection temperature is maintained at about T_{cell} = 300 K.

TABLE 1. Design Parameters and Ranges for a Radioisotope Power System with TPV.

Parameter	**Values and Ranges**			
Number of sides with TPV converter	1	**2**	4	(baseline design in boldface)
Area of TPV cells, A_{array} (cm^2)	100	**200**	400	cm^2
Input heat flux, P_{in} (W/cm^2)	1.25	**2.50**	5.00	W/cm^2
Emitter temperature, T_e (K)	~1200 K to 1350 K (≅ aeroshell temperature)			
Emissivity of surface, $\varepsilon_s(\lambda)$	Depends upon material selected			
Reflectance of filter, $R_f(\lambda)$	• ~0.1 below TPV cell cutoff wavelength • ~0.9 above TPV cell cutoff wavelength			
Band-gap of TPV cell, E_g (eV)	• 0.6 eV (cutoff wavelength 2.07 microns) to • 0.74 eV (cutoff wavelength 1.68 microns)			
Quantum efficiency of TPV cell, $QE(\lambda)$	Measured data as a function of wavelength			
Cell temperature, T_{cell} (K)	~275 to 350 K			

The selection of particular radiant emitter, TPV cell, and filter component hardware determines the characteristics such as emittance of the radiant surface $\varepsilon_s(\lambda)$, the reflectance of the filter $R_f(\lambda)$, and the quantum efficiency of the TPV cells $QE(\lambda)$ for a particular band-gap E_g (eV). Figure 4 shows the spectral characteristics for the specific hardware used in the tests described in this paper. The hardware selections for the test include:

- TPV cells. The TPV cells are InGaAs on InP substrates with a band-gap E_g = 0.60 eV. Murray, *et al*. (2004) describe the structure of these TPV cells. The cells are 2.3 cm by 2.3 cm overall (Figure 5). The cells use a Monolithic Integrated Module (MIM) structure and have 25 interconnected diodes on each MIM. Each cell incorporates an anti-reflection coating (ARC) on the front side and a gold Back Surface Reflector (BSR). Figure 4 shows the quantum efficiency for these TPV cells. Note that the band-edge for the tandem filter and the band-gap of the TPV cells are matched at a wavelength of 2.07 microns. These cells have excellent performance, with a fill factor of 0.65 or more and a dark current density of 1x10^{-6} A/cm^2.

- A tandem plasma/dielectric filter. The tandem filter is comprised of a multilayer dielectric interference filter coating (by Rugate Technologies, Inc.) on a substrate coated with the plasma filter (by Emcore Corporation). The dielectric filter is comprised of multiple layers of high index of refraction material (Sb_2Se_3) and low index of refraction material (YF_2). The plasma layer is InPAs on an InP substrate. DePoy, *et al*. (2004) describe these filters and their performance in the context of spectral control for TPV. The spectral reflectance is measured by Rugate Technologies is shown in Figure 4. The filter has very low reflectance (~0.1) in the range of wavelengths (<2.07 microns) convertible to electric power by the TPV cells, and very high reflectance in the range of wavelength (>2.07 microns) not convertible by the TPV cells.

- A graphite plate for the radiant emitter. The graphite plate is a block of commercial graphite material (Poco Graphite Type DFP-1). The surface area is 100 cm^2 in the optical cavity. The spectral emittance of the graphite plate (Figure 4) has been measured with spectrophotometer equipment at NASA Glenn Research Center.

For the tests, 16 cells are mounted on a cooling plate (Figure 6a). Four cells are connected in series to form four strings. The array of cells occupies 82 cm^2 (82%) of the surface area. The remainder of the surface (18%) is plated with gold, with a reflectance of 0.98 or better. Electrical connections permit the current and voltage to be measured individually for each of the four strings. Tandem filter components are cut to cover two TPV cells simultaneously. The filter components are then mounted over the TPV cells using an optical adhesive (Figure 6b). As discussed by Murray, *et al*., 2004, it is important to match the band-edge of the TPV cells with the filters in laying out the array.

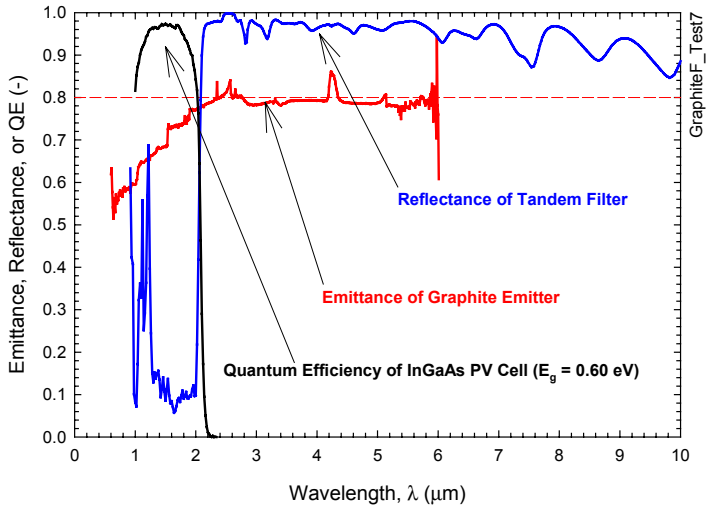

FIGURE 4. Spectral Characteristics of Radiant Emitter, Tandem Filter, and TPV Cell Components.

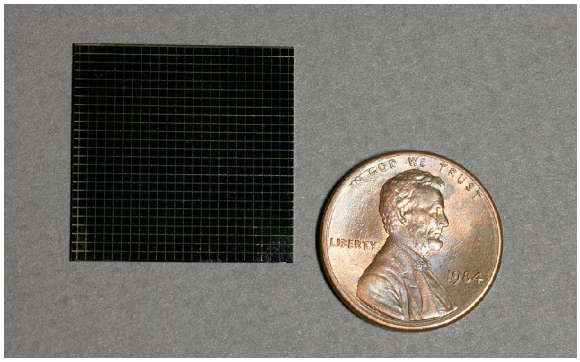

FIGURE 5. MIM Structure with 25 Diodes for InGaAs Cell at E_g = 0.60 eV (2.3 cm by 2.3 cm Cell).

(a) Without Tandem Filter (b) With Tandem Filter

FIGURE 6. 4x4 Array of TPV Cells (Four Strings of Four Cells Connected in Series).

TEST APPARATUS

The test facility (Figure 7) includes the following key components:

- Vacuum vessel (10^{-6} torr vacuum pressure)
- Diffusion and roughing pumps
- Chiller for cooling the plates upon which the TPV cells are mounted
- Voltage controllers for heaters (up to 2000 W_t heat input with flat-plate electrical heaters)
- Resistor bank for TPV cell output power (to map current *vs*. voltage)
- Passthroughs for instrumentation and controls
- DAS system with LabVIEW® software

The TPV test article (Figure 8) is placed in this thermal vacuum chamber for testing. The TPV cell arrays are installed in close proximity (2 mm spacing) to the emitter surface to form an optical cavity bounded by the emitter, the cooling plate with mounted PV array (Figure 6), and a tantalum foil at the perimeter of the gap between the two.

The tests include parasitic losses in the optical cavity that are representative of arrays for the RTPV converter. These heat transfer losses can occur in various locations: at the boundary of the gap between the emitter and the TPV cell/filter surface, to the gold-coated surface in the area not covered by TPV cells, and to the edges of the cells (≅1 mm thick) because they are not mounted flush with the surface.

Thin tantalum foils bound the gap between the emitter and the TPV cell arrays. The tantalum foils prevent direct loss of input power by blocking radiation out of the optical cavity, except for a very small area at each corner of the cavity. The tantalum foils are attached to the graphite plate serving as the emitter, and they are at the temperature of the emitter. Their surface area is about 10 cm^2 in the optical cavity, or about 10% of the emitter surface area. These tantalum foils are polished, and the emissivity of the surface is ≅0.3 in the optical cavity. Where the tantalum foils contact the mounting plate, the foils have a knife-edge with low contact pressure to minimize heat transfer losses due to thermal conduction. Tests with gold-coated plates in place of the TPV cell array confirm the low heat transfer losses due to thermal conduction.

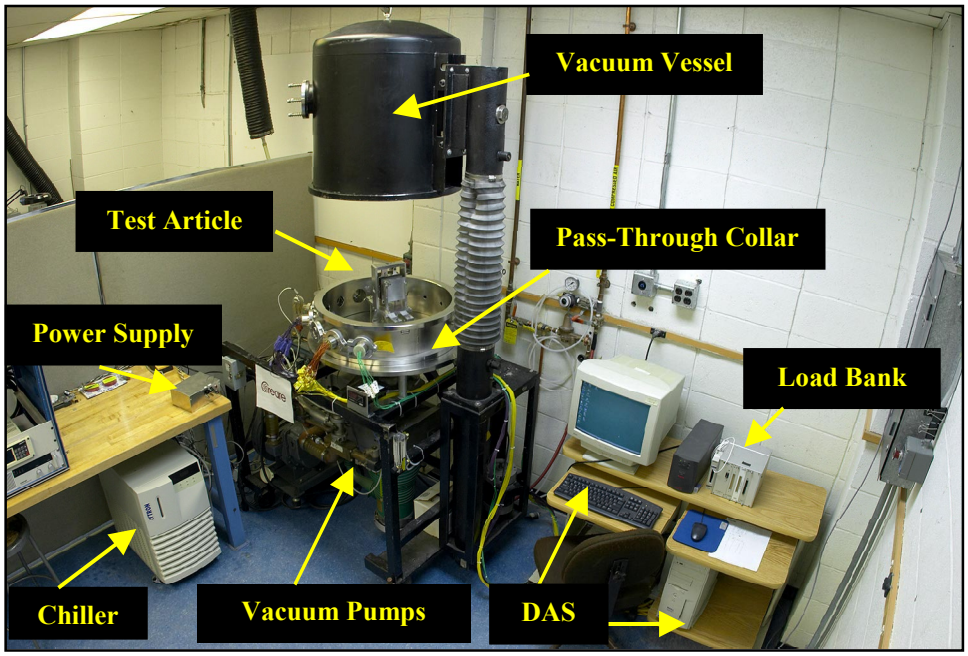

FIGURE 7. Photograph of Test Facility with Vacuum Chamber.

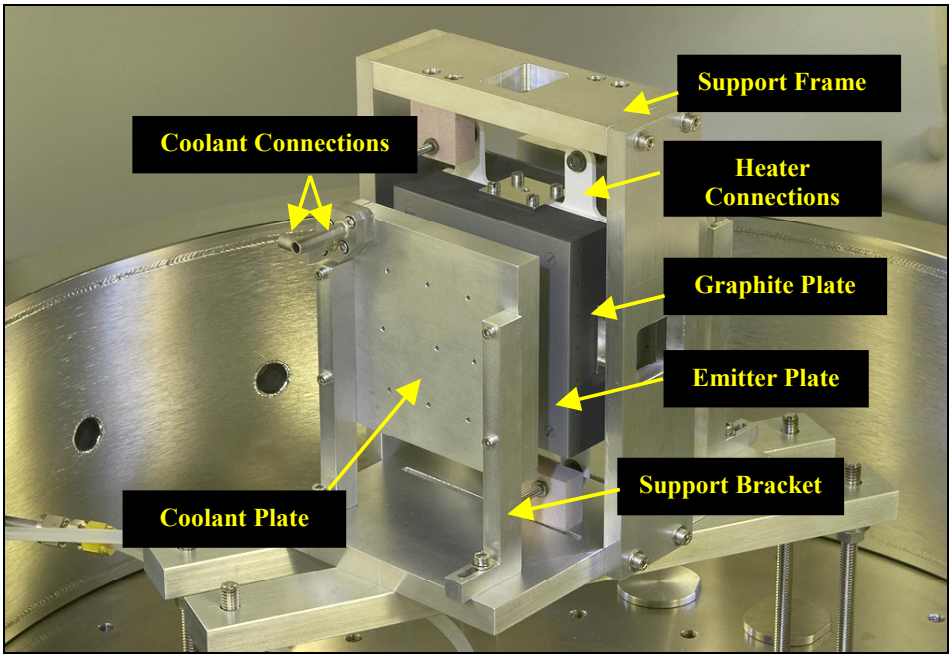

FIGURE 8. Photograph of Test Article (Without Insulation or Tantalum Foils).

TPV PERFORMANCE WITH A FILTERED ARRAY

Test Data. Figure 9 shows the measured results for the test configuration:

- A 4x4 array of E_g = 0.60 eV TPV cells, or 16 cells with a total (prototypical) area of 82 cm^2.
- Tandem plasma/dielectric filter components matched to the TPV cells.
- A graphite emitter with spectral emittance $\varepsilon \cong 0.8$.

Data include the electrical power output (filled circles in Figure 9a), heat load to the cooling plate (filled squares in Figure 9a), and conversion efficiency for the array (filled circles in Figure 9b). The key results are:

- At 1330 K, the electrical power output is 54.4 W (Figure 9a) and the conversion efficiency is $\eta_{array} \cong 19.1\%$ (Figure 9b).
- Heat load in the cavity and power output at 1350 K (Figure 9a) are close to the target values for a 500 W_t RPS (Figure 1).
- All measured results follow the trends with temperature calculated by the analytical model (solid lines in Figure 9); comparisons between the measured data and an analytical model are very good.

The temperature of the radiant emitter, T_e, is measured with two Type B thermocouples inserted into the graphite block used as the emitter in these tests. The uncertainty is ±2 K.

The electrical power output P_{out} (filled circles in Figure 9a) is the sum of the maximum electrical power output P_{mp} from all Strings 1, 2, 3, and 4:

$$P_{out} = (P_{mp1} + P_{mp2} + P_{mp3} + P_{mp4}) \tag{5}$$

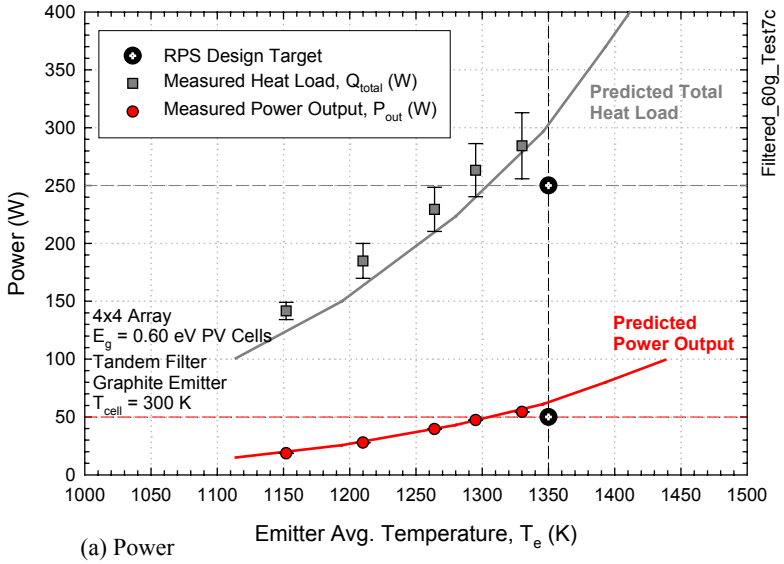

(a) Power

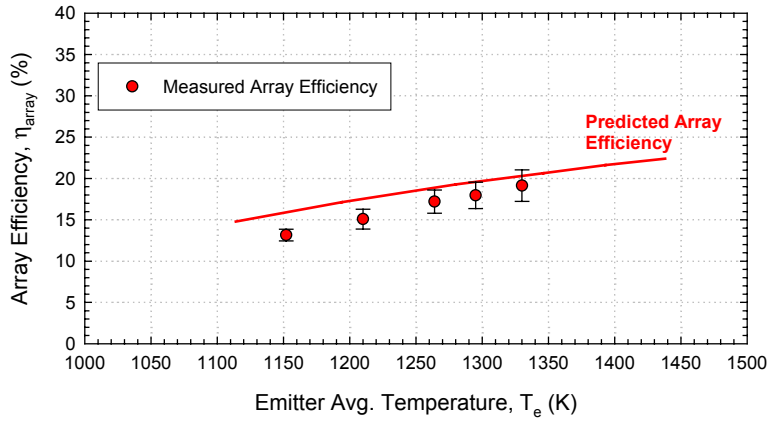

(b) Efficiency

FIGURE 9. Performance of 4x4 TPV Cell Array with Tandem Filter.

For each of the four strings in the array, the current versus voltage characteristic (Figure 10, for String 4) is measured at steady-state test conditions by adjusting a variable resistor. The combination of current and voltage that provides the maximum output power (filled circles in Figure 10) is found for each string and summed to get the total electrical power output. Figure 11 compares the intercepts on the y-axis (short-circuit current I_{sc}) and x-axis (open circuit voltage V_{oc}) as a function of emitter temperature. Increased radiant heat transfer above the cell band-gap at higher emitter temperature rapidly leads to larger power output, which manifests as larger current. The open-circuit voltage is less sensitive to the temperature and is only slightly greater when the emitter temperature is larger. (Although not shown here, the voltage also varies about ±0.2%/K with TPV cell temperature.) The values and trends of the measured voltage and current data compare well with the analytical model. The fill factor parameter is the ratio of the maximum power output P_{mp} to the theoretical limit on the power output given by the product $V_{oc}I_{sc}$. Figure 11 shows that the fill factor from the experimental measurements agrees with the characteristic value of FF = 0.65 as measured for the individual TPV cells. The larger the fill factor, the better the TPV cells perform. The TPV cells provided by Emcore for this project have outstanding performance.

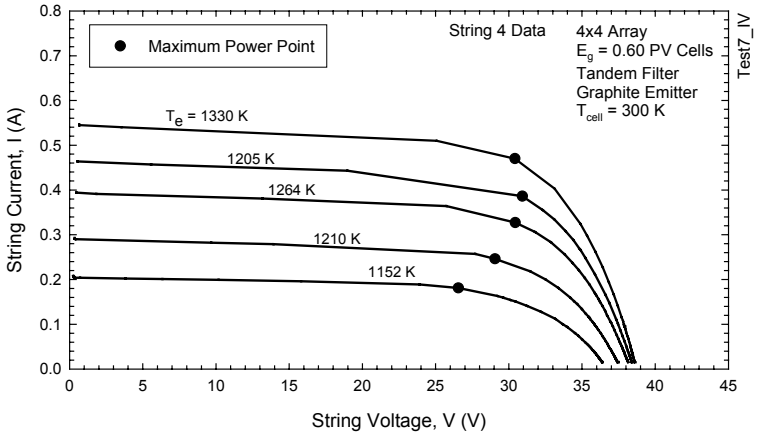

FIGURE 10. Measured Current vs. Voltage Data from TPV Cell Strings for 4x4 Array With Tandem Filter.

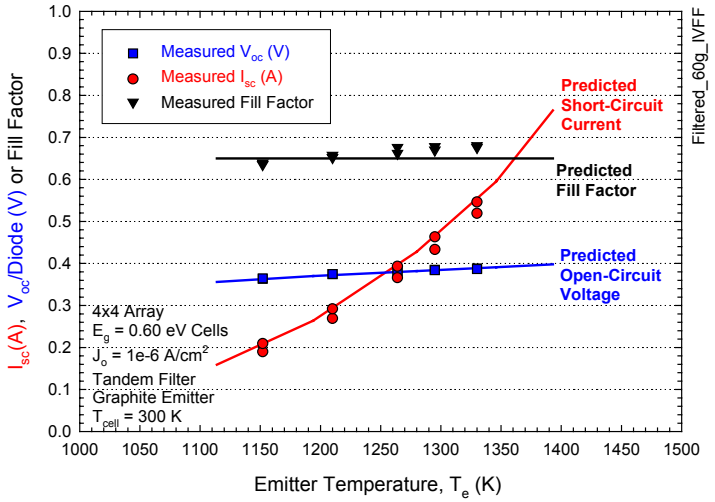

FIGURE 11. Measured Short-Circuit Current (I_{sc}), Open-Circuit Voltage (V_{oc}), and Fill Factor for 4x4 Array with Tandem Filter.

The total heat load Q_{total} on the coolant plate from the radiant heat transfer in the optical cavity (gray squares in Figure 9a) is:

$$Q_{total} = [P_{out} + (m_w c_p \Delta T) - Q_{external}] \tag{6}$$

where P_{out} is the electrical power output above, the $(m_w c_p \Delta T)$ term is the heat load to the cooling plate measured by a heat balance on the coolant stream (water), and $Q_{external}$ is a parasitic heat addition term. The cooling plate includes internal coolant passages. In these tests, some of the heat that the coolant plate receives does not arrive from the optical cavity. It arrives via external radiation heat transfer from the hot surfaces to the cold plate, or by thermal conduction through the mechanical supports. These effects are a consequence of the test set-up used, and are not prototypical. We quantify this heat gain on the coolant plate by a calibration test using a gold plate in place of the test article so that the total load from the optical cavity is small. $Q_{external}$ = 30 to 45 W over the range of temperatures tested. Thermal conduction through the support brackets (see Figure 8) accounts for about one-third of this.

The conversion efficiency of the array (filled circles in Figure 9b) is then just:

$$\eta_{array} = \left[\frac{P_{out}}{Q_{total}} \right] \tag{7}$$

This determines the result $\eta_{array} \cong 19.1\%$ at $\cong 1350$ K. Without the correction $Q_{external}$, the conversion efficiency would still be $\eta_{array} \cong 16.5\%$.

Uncertainty bands for the measured data points are displayed in Figure 9. A method for calculating the measurement uncertainty for single-sample experiments (Kline and McClintock, 1953) is used to estimate the uncertainty. The uncertainty in a quantity R is given by:

$$\delta R(X_1, X_2 \ldots X_n) = \left\{ \sum_{i=1}^{n} \left[\left(\frac{\partial R}{\partial X_i} \right) \delta X_i \right]^2 \right\}^{0.5} \tag{8}$$

The quantity R in this case could be the emitter temperature T_e, the power output P_{out}, the total heat load Q_{total}, or the array efficiency η_{array}. These parameters may be either directly measured (such as the emitter temperature) or derived from other measurements (X_1, X_2, …X_n). Table 2 lists the uncertainties in the measured quantities.

TABLE 2. Uncertainties in Measured Test Parameters.

Measured Parameter	Measurement Uncertainty
Emitter temperature, T_e	±2 K
String current at maximum power, I_{mp}	±0.00012 A
String voltage at maximum power, V_{mp}	±0.078 V
Coolant mass flow rate, m_w	±0.00315 kg/s
Coolant outlet or inlet temperature, T_{wout} or T_{win}	±0.2 K

The uncertainty band is very small for the electrical power output, since the current and voltage can be measured with high accuracy. The uncertainties in heat load and efficiency are dominated by the uncertainty in the measured temperature difference (ΔT) for coolant flowing into and out of the coolant plate upon which the TPV cell array is mounted. The flow rate for this coolant is large, so that the temperature is uniform across the coolant plate and the TPV cell array.

Analyis. Performance has also been estimated analytically. We first developed detailed two-dimensional and three-dimensional thermal models of the TPV converter using the FLUENT™ software. Various parasitic losses can be calculated using this detailed model. Results from two-dimensional (2-D) model calculations are shown as the solid lines in Figure 9. Spectral emittance characteristics as measured for the test hardware (Figure 4) are used as boundary conditions in the model. The temperatures and heat fluxes from this thermal model are then used as inputs to a spreadsheet analysis that calculates the power output from the TPV cells. Measured characteristics of the TPV cells are used in this model. To understand the analysis of TPV performance, the interested reader may refer to the technical paper by Schock, Or, and Mukunda (1996) for a first-order, one-dimensional model.

The analytical results indicate that the spectral efficiency $\eta_{spectral} \cong 0.8$, and the cavity efficiency due to parasitic losses in the optical cavity is $\eta_{cavity} \cong 0.9$ at 1350 K. The network efficiency is estimated to be $\eta_{network} \cong 0.98$. With a measured TPV cell efficiency of $\eta_{PVcell} = 0.28$, this gives the predicted overall array conversion efficiency of $\eta_{array} \cong 0.20$ which is very close to the measured result ($\eta_{array} \cong 0.19$).

With the tantalum foils providing a very good boundary at the edge of the cavity, the main parasitic losses are absorption of radiant energy by the edges of the TPV cells and the highly reflective gold coating. The TPV cells protrude from the surface. Absorption at the edges of the cells (and filters) accounts for three-fourths of the parasitic loss in the optical cavity. This suggests that if the array is mounted so that the surface of the filters is flush with the gold surface surrounding the array, then the efficiency of the optical cavity could be as high as $\eta_{cavity} \cong 0.97$. Although not possible here, this straightforward modification alone would improve the array efficiency to $\eta_{array} \cong 0.20$.

SUMMARY OF TPV PERFORMANCE DATA

Table 3 summarizes the results of the TPV performance measurements for cells and arrays using the filters and TPV cells described in this paper. These test results include the TPV cell performance, spectral control, cavity losses, and network/array losses. The TPV array efficiency at 1350 K is 19% with tandem filters. In tests with single cells and tandem filters, which therefore include cell power conversion efficiency and spectral efficiency factors, the TPV conversion efficiency is 25% (Wernsman, *et al.*, 2005). (Siergiej, *et al*., 2002 describe the test set-up and procedure for the single-cell tests.) Those single-cell tests do *not* include parasitic losses in a prototypical optical cavity or network losses, like the array tests described in this paper.

Recently, Brown, *et al*. (2004) report that the efficiency of a 100 cm^2 array of filtered TPV cells is 12.4%, when the array is comprised of TPV cells having a single-cell efficiency of 15%. The progression from single-cell results to filtered arrays of cells at similar array size is consistent with the present results.

We have performed tests on a 4x4 array that does not include the filters on the TPV cells. In those tests, the measured array efficiency is $\eta_{array} \cong 0.10$, compared with $\eta_{array} \cong 0.19$ for cells with a tandem filter. Without a filter, the spectral efficiency of the TPV cells is only $\eta_{spectral} \cong 0.50$, while it is $\eta_{spectral} = 0.80$ with the tandem filters. Comparison of these results illustrates the significant benefit of the spectral control provided by the filters. Note that if it is desired to use TPV cells without tandem filters for some application, the spectral efficiency of the cells could be improved to about $\eta_{spectral} \cong 0.60$. The cells used here were optimized to perform best with the tandem filter.

The present test results do not include parasitic losses associated with a housing or DC power regulation. We estimate that the efficiency of the housing (ratio of heat reaching the radiant emitter to the power supplied from the GPHS heat source) should be about 0.90, and the efficiency of DC-to-DC power regulation should be 0.98.

Table 4 summarizes the breakdown of measured and estimated efficiency factors for a 500 W_t RPS with the configuration shown in Figure 1. The net conversion efficiency, based upon these data is 17% with current technology. With an estimated mass of 7.1 kg (including radiators not shown in Figure 1), the specific power for the RPS would be 12 W_e/kg. The conversion efficiency and specific power of an RPS with TPV power conversion would be about two-and-a-half times that of an RTG at the beginning of a mission, using present TPV components. With improvements in cell performance, we estimate that a factor of 1.15 improvement in efficiency is possible.

TABLE 3. TPV Performance Measurements for TPV Cells and Arrays (T_e = 1350 K; T_{cell} = 300 K).

Technology E_g = 0.60 eV TPV Cell (High-Doping LCL)	**Single-Cell Results w/White Light Source[1]** η_{PVcell}	**Single-Cell Results With Emitter & Spectral Control[2]** $(\eta_{spectral}) \times (\eta_{PVcell})$	**Array Results With Optical Cavity (16 Cells)** $\eta_{array} = (\eta_{cavity}) \times (\eta_{spectral}) \times (\eta_{PVcell}) \times (\eta_{network})$
Tandem Filter	28%	25%	19%
ARC Only	28%	15%	10%

[1]Measurements performed in test facilities at Emcore Corporation (Murray, *et al*., 2004).
[2]Measurements performed in test facilities at Bechtel Bettis Laboratories.

TABLE 4. Estimates of TPV Performance for a 500W_t RPS.

Generator Level	**Efficiency Factor**	**Current Basis**	**Current Value**	**Future Value**
Cells Only	η_{PVcell}	Measured Data	0.28	0.32
Filtered Cells	$\eta_{spectral}$	Measured Data	0.8	0.8
Cell Arrays	η_{cavity}	Measured Data	0.9	0.9
Cell Arrays	$\eta_{network}$	Measured Data	0.98	0.98
Generator	$\eta_{housing}$	Estimated Analytically	0.9	0.9
Generator	$\eta_{DCcontrol}$	Estimated Analytically	0.98	0.98
Total	η_{RTPV}	Estimated Analytically	0.17	0.20
	Output Power	Estimated Analytically	**85 W_e**	**100 W_e**
	Mass	Estimated Analytically	**7.1 kg**	**7.1 kg**
	Specific Power	Estimated Analytically	**12 W_e/kg**	**14 W_e/kg**

CONCLUSION

Test data for a TPV converter at prototypical size for an RPS show that the array conversion efficiency is 19% at the operating temperature of 1330 K on the hot side and 300 K for heat rejection. This result was accomplished with existing technology for a radiant emitter, tandem plasma/dielectric filters for spectral control, and a 4x4 array of high-performance TPV cells (InGaAs MIMs at E_g = 0.60 eV). These tests include the largest factors affecting the conversion efficiency: cell electrical conversion, spectral control, and parasitic heat losses in the optical cavity. The results extrapolate to a conversion efficiency of 17% when other parasitic losses (between the GPHS and the radiant emitter) and DC-to-DC power regulation are included. This corresponds to a specific power of 12 W_e/kg for a 100 W_e RPS. With existing technology then, TPV conversion can achieve conversion efficiency and specific power about 2.5 times greater than an RTG at the Beginning of Mission. Factors affecting the power output over mission lifetime are being studied.

NOMENCLATURE

A_{array}	=	area of TPV cell array (cm^2)
E_g	=	band-gap of TPV cell (eV)
c_p	=	heat capacity of the water (4200 J/kg-K)
I_{mp}	=	current in PV cell string at maximum electrical power output (A)
I_{sc}	=	short-circuit current (A)
J_o	=	dark current density (A/cm^2)
m_w	=	mass flow rate of the coolant (kg/s)
P_{emit}	=	total emitted power (W)
P_{in}	=	net emitted power (W or W/cm^2)
P_{mpn}	=	maximum electrical power output from string (W), where n = 1, 2, 3, or 4
P_{out}	=	total electrical output power from TPV cells (W)
P_{reject}	=	power to converter heat rejection (W)
$P_{reflect}$	=	power reflected by spectral control filter (W)
QE	=	quantum efficiency of TPV cell
$Q_{external}$	=	heat load to PV array cooling plate from external sources (W_{th})
Q_{total}	=	total load on coolant plate in TPV performance test (W_{th})
R	=	arbitrary quantity in uncertainty analysis
R_f	=	reflectance of tandem filter
T_e	=	emitter temperature (K)
T_{cell}	=	TPV cell (or heat rejection) temperature (K)
ΔT	=	the temperature difference in the coolant (T_{wout}-T_{win}) (K)
T_{wout}	=	measured coolant temperature at the outlet (K)
T_{win}	=	measured coolant temperature at the inlet (K)
V_{mp}	=	open-circuit voltage of PV cell string at maximum electrical power output (V)
V_{oc}	=	open-circuit voltage (V)
X_i	=	value of measured quantity used in uncertainty analysis
ε_s	=	emissivity of radiant surface
λ	=	wavelength (microns)
λ_c	=	cutoff wavelength (microns)
η_{RTPV}	=	overall RTPV conversion efficiency
$\eta_{housing}$	=	efficiency of the housing (includes parasitic heat losses in supports and insulation)
η_{cavity}	=	efficiency of the optical cavity (includes parasitic heat losses)
$\eta_{spectral}$	=	efficiency at the TPV cell surface (ratio of energy at E > E_g and total energy)
η_{PVcell}	=	efficiency of the power conversion of a TPV cell (including active area fraction)
$\eta_{network}$	=	efficiency of the array of TPV cells, including losses from series/parallel connection and non-uniform illumination in the optical cavity
$\eta_{DCcontrol}$	=	efficiency of the power electronics that provide regulated 28 V DC output
η_{array}	=	efficiency of TPV cell array (product of η_{PVcell}, $\eta_{spectral}$, η_{cavity}, and $\eta_{network}$)

ACKNOWLEDGMENTS

This work was performed under the guidance and support of NASA under Contract NAS3-03117. Any opinions, expressed or implied, are those of the authors. We would also like to thank the System Assessment Team for their technical comments and discussions. Members of the project team who contributed to this technical effort included: Emcore Corporation, NASA Glenn Research Center, Polytechnic University, Oak Ridge National Laboratory, Rugate Technologies Incorporated, and Naval Research Laboratory. The project team would also like to express their appreciation to Bechtel Bettis Inc. and Knolls Atomic Power Laboratory for their willingness to participate in technical discussions.

REFERENCES

Brown, E.J., Baldasaro, P.F., Burger, S.R., Danielson, L.R., DePoy, D.M., Dolatowski, J.M., Fourspring, P.M., Nichols, G.J., Topper, W.F., and Rahmlow, R.D.; "The Status of Thermophotovoltaic Energy Conversion Technology at Lockheed Martin Corp.," AIAA 2004-5676, 2nd Int. Energy Conversion Engineering Conference, Providence, R.I., 2004.

DePoy, D.M., Fourspring, P.M., Baldasaro, P.F., Beausang, J.F., Brown, E.J., Dashiell, M.W., Rahner, K.D., Rahmlow, T.D., Lazo-Wasem, J.E., Gratrix, E.J., and Wernsman, B.; "Thermophotovoltaic Spectral Control," AIAA 2004-5762, 2nd International Energy Conversion Engineering Conference, Providence, R.I., 2004.

DePoy, D.M., Brown, E.J., Baldasaro, P.F., Rice, L.P., and Rahmlow, T.D., "Radioisotope Powered Thermophotovoltaic Energy Systems," in *Proceedings of Space Technology and Applications International Forum (STAIF-2003)*, edited by M. El-Genk, AIP Conference Proceedings 654, New York, 2003, pp. 1-11.

Fraas, L.M., Avery, J.E., Huang, H.X., and Martinelli, R.U., "Thermophotovoltaic System Configurations and Spectral Control," *Semiconductor Science and Technology*, **18**, S165-S173 (2003).

Kline, S.J. and McClintock, F.A.; "Describing Uncertainties in Single Sample Experiments," *Mechanical Eng*., January, 1953, pp. 3-8.

Loughlin, S., and Uppal, P., "Radioisotope Thermophotovoltaic Generator For Space Power Applications," IECEC Paper No. AP-302, in *Proceedings of the 30th Intersociety Energy Conversion Engineering Conference*, Vol. 1, edited by D.Y. Goswami, *et al*., New York, August, 1995, pp. 657-660.

Murray, C.S., Crowley, C.J., Murray, S., Elkouh, N.A., Hill R.W., and Chubb, D.L.; "Thermophotovoltaic Converter Design for Radioisotope Power Systems," in *Proceedings of the 6th Conference on Thermophotovoltaic Generation of Electricity*, edited by J. Luther, *et al.*, AIP Conference Proceedings, New York, 2004, to be published.

Schock, A., Or, C., and Mukunda, M., "Effect of Expanded Integration Limits and of Measured Infrared Filter Improvements on Performance of RTPV System," in *Proceedings of the 2nd NREL Conference on Thermophotovoltaic Generation of Electricity*, edited by J. Benner, *et al.*, AIP Conference Proceedings 358, New York, 1996, pp. 55-80.

Schock, A., Or, C. and Kumar, V., "Modified Design of Radioisotope Thermophotovoltaic Generator to Mitigate Adverse Effect of Measured Cell Voltage," in *Proceedings of the 31st Intersociety Energy Conversion Engineering Conference*, IEEE Catalog No. 96CH35878, Vol. 2, edited by P. Chetty, *et al*., New Jersey, 1996, pp. 979-986.

Schock, A. and Or, C., "Effect of Updated Data Base and Improved Analysis on Performance of Radioisotope Thermophotovoltaic Converter," in *Proceedings of the 31st Intersociety Energy Conversion Engineering Conference*, IEEE Catalog No. 96CH35878, Vol. 2, edited by P. Chetty, *et al*., New Jersey, 1996, pp. 987-994.

Siergiej, R.R., *et al*., "20% Efficient InGaAs/InPAs Thermophotovoltaic Cells," in *Proceedings of the 5th NREL Conference on Thermophotovoltaic Generation of Electricity*, ed. T. Coutts, *et al.*, AIP Conference Proceedings 653, New York, 2002.

Vicente, F.A., Kelly, C.E., and Loughlin, S., "Thermophotovoltaic (TPV) Applications to Space Power Generation," IECEC Paper No. 96278, in *Proceedings of the 31st Intersociety Energy Conversion Engineering Conference*, IEEE Catalog No. 96CH35878, Vol. 1, edited by P. Chetty, *et al*., New Jersey, August, 1996, pp. 635-640.

Wernsman, B., *et al.*, "Advanced Thermophotovoltaic Devices for Space Nuclear Power Systems," in these proceedings, *Space Technology and Applications International Forum-2005,* ed., El-Genk, *et al.*, AIP Conference Proceedings, New York, 2005.